

Design of Vacuum Post-Drying Procedures for Electrodes of Lithium-Ion Batteries

Fabienne Huttner,^{*[a, b]} Axel Marth,^[a, b] Jochen C. Eser,^[c] Thilo Heckmann,^[c] Jonas Mohacsi,^[c] Julian K. Mayer,^[a, b] Philip Scharfer,^[c] Wilhelm Schabel,^[c] and Arno Kwade^[a, b]

In order to reduce the residual moisture in lithium-ion batteries, electrodes and separators need to be post-dried prior to cell assembly. On an industrial scale, this is often conducted batch-wise in vacuum ovens for larger electrode and separator coils. Especially for electrodes, the corresponding post-drying parameters have to be carefully chosen to sufficiently reduce the moisture without damaging the sensitive microstructure. This requires a fundamental understanding of structural limitations as well as heat transfer and water mass transport in coils. The aim of this study is to establish a general understanding of the vacuum post-drying process of coils. Moreover, the targeted

design of efficient, well-adjusted and application-oriented vacuum post-drying procedures for electrode coils on the basis of modelling is employed, while keeping the post-drying intensity as low as possible, in order to maintain the sensitive microstructure and to save time and costs. In this way, a comparatively short and moderate 2-phase vacuum post-drying procedure is successfully designed and practically applied. The results show that the designed procedure is able to significantly reduce the residual moisture of anode and cathode coils, even with greater electrode lengths and coating widths, without deteriorating the sensitive microstructure of the electrodes.

1. Introduction

In the long and complex process chain of lithium-ion batteries (LIBs), the post-drying step constitutes an important, improvable step with regard to its significant influence on the safety and cycling stability of the cells as well as its high energy costs. Post-drying usually takes place directly before cell assembly or cell closure, depending on the chosen cell format and process route. It aims at reducing the residual moisture in the cell components below a critical level to ensure a long battery cell life and high safety. On an industrial scale, post-drying is most commonly conducted either in continuous roll-to-roll processes, where the electrodes or separators are often heated by infrared emitters, or batch-wise by post-drying whole coils in vacuum ovens.^[1–5]

In this study, batch-wise post-drying of coils in a vacuum oven is investigated. The batch post-drying of entire coils has many advantages. In contrast to roll-to-roll-processes or post-

drying of punched-out electrodes, post-drying in vacuum ovens enables parallelized post-drying of a multitude of electrode and/or separator coils at the same time. At industrial scale, multiple coils with several hundred meters length can be post-dried at the same time, requiring minimal space and no control or adjustments by the staff. Additionally, it offers the advantages of easy transport, storage and protection of the cell components, due to lack of unrolling, and finally higher water diffusion coefficients compared to atmospheric drying. Disadvantages are the slow heating of whole coils and, concerning the electrodes, very long diffusion paths, as the moisture can only diffuse in axial direction out to the sides along the coating of the electrodes.^[2,6] To overcome these restrictions, vacuum post-drying processes have to be well-adjusted to the respective material systems and coil dimensions. As this requires a profound understanding of the process and the implementation of preliminary studies, post-drying processes are often oversized. This leads to the following disadvantages: Firstly, higher costs are caused due to higher energy consumption and unnecessary long processing times, the latter leading to a decelerated production.^[4] Secondly, higher temperatures and/or longer processing times can damage the electrode microstructures and deteriorate the cell performance.^[1] However, it is impractical and inefficient to design an individual post-drying procedure for every single application. Instead, procedures are needed that can be applied for a certain range of applications without being appreciably under- or oversized. This enables post-drying of electrode coils with slightly different compositions or different geometries in parallel while maintaining the same post-drying procedure, even if small changes are made in upstream processes.

[a] F. Huttner, A. Marth, J. K. Mayer, Prof. Dr.-Ing. A. Kwade

Institute for Particle Technology

Technische Universität Braunschweig

Volkmaroder Straße 5, 38104 Braunschweig, Germany

E-mail: fabienne.huttner@tu-bs.de

[b] F. Huttner, A. Marth, J. K. Mayer, Prof. Dr.-Ing. A. Kwade

Battery LabFactory Braunschweig

Technische Universität Braunschweig

Langer Kamp 19, 38103 Braunschweig, Germany

[c] J. C. Eser, T. Heckmann, J. Mohacsi, Dr.-Ing. P. Scharfer, Prof. Dr.-

Ing. Dr. W. Schabel

Karlsruhe Institute of Technology

Thin Film Technology

Straße am Forum 7, 76131 Karlsruhe, Germany

 © 2021 The Authors. *Batteries & Supercaps* published by Wiley-VCH GmbH. This is an open access article under the terms of the Creative Commons Attribution License, which permits use, distribution and reproduction in any medium, provided the original work is properly cited.

1.1. Residual Moisture and Post-Drying of LIBs

Despite still not having been investigated adequately, the post-drying step plays a particularly important role as moisture represents a critical contamination in LIBs. First of all, residual moisture can lead to unwanted side reactions with the conducting salt LiPF₆ of the electrolyte. The side reactions cause the formation of gaseous hydrogen fluoride (HF) and other acidic decay products, which has many negative influences on the cell.^[1,7–11] The loss of the conducting salt reduces the conductivity and increases the internal cell resistance. This leads to a deterioration of the cell performance. Cell safety is affected by increased internal cell pressure, caused by the formation of gaseous hydrogen fluoride, as high internal cell pressure can lead to cell bursting. In addition, the acidic hydrogen fluoride can promote decomposition and corrosion of the active materials.^[12–14] The compounds resulting from high residual moisture contents can impede the formation of a stable solid electrolyte interface (SEI), which protects the anode against the electrolyte, or affect an already existing SEI. This leads to a lower cycling stability.^[12,15–18]

However, it was also shown that small amounts of moisture can have a positive impact. In their study about water uptake of LFP (LiFePO₄) and NCM (Li(Mn_{0.37}Co_{0.35}Ni_{0.35}O_{2.07}) cathodes, Langlotz et al.^[13] stated that small amounts of moisture on the cathode's side seem to enhance the formation of a stable SEI in cells with graphite anodes. It has also been shown that residual moisture (25–50 ppm) in LiPF₆-based electrolytes can lead to more homogenous SEIs on deposited lithium electrodes.^[19] Logan et al.^[20] discovered that LFP/graphite cells tolerated moistures of ca. 500 ppm when the electrolyte contained additives such as vinylene carbonate (VC). In previous studies focusing on single compartment pouch cells with a NCM622 cathode, a graphite anode and Separion® S240P30 as separator, a good cell performance was achieved by reducing the residual moisture content in the cells to about 300 ppm (calculated for cathode, anode and separator according to their mass ratios, current collectors included).^[1]

Although it has a high impact on cell performance and safety, the post-drying step has not been sufficiently investigated until today. As reported in literature, there is a lack of research concerning the post-drying step and its influence on structural and electrochemical properties.^[21] In addition, the sensitivity of the electrodes towards higher post-drying intensities is strongly dependent on the chosen material system, especially the binders. Hence, findings for differing material systems are only partly transferable or comparable. In general, very different approaches can be found concerning the post-drying parameters for LIB cell components, while detailed information is often hard to find: Yamaki et al.^[22] post-dried graphite anodes with PVDF binder for 12 hours at 70 °C under vacuum. Li et al.^[23] chose 2 hours and 100 °C for NCM532 cathodes with PVDF binder. Liu et al.^[24] indicated that they post-dried graphite anodes with CMC binder for 12 hours at 80 °C under vacuum. Liu et al.^[25] chose 120 °C for post-drying both NCM cathodes with PVDF and graphite anodes with PVDF, but did not provide details about vacuum level or post-drying

time. Logan et al.^[26] stated that they post-dried LiFePO₄/artificial graphite cells for 14 hours between 100 °C and 120 °C under vacuum. Prietzl et al.^[27] post-dried graphite anodes with PVDF and NCM851005 cathodes with PVDF for 12 hours at 120 °C under dynamic vacuum. In addition, they investigated temperatures of 80 °C, 180 °C and 300 °C for drying steps (before final post-drying) after washing nickel-rich cathodes, and detected that the drying temperature is a critical step for Ni-rich NCM, as the specific discharge capacities dropped steeply with increasing temperature. Komaba et al.^[28] post-dried graphite anodes with PVDF overnight at 80 °C under vacuum. Haarmann et al.^[29] chose 16 hours and 120 °C in vacuum for graphite anodes and NCM622 cathodes with PVDF binder.

As the research results show, post-drying parameters differ from 70 to 120 °C and from 2 to 16 hours. In a previous study about the influence of different post-drying procedures on remaining moisture and physical and electrochemical properties of LIBs^[1], it was shown that a good cell performance can not only be guaranteed by low residual moisture but also, in particular, by gentle post-drying. The best cell performance was achieved by a very mild Argon post-drying (20 °C/15 min/3 Vacuum-Argon purging cycles), whereas post-drying for 18 hours at 120 °C under vacuum already led to the deterioration of structural and electrochemical properties. However, the Argon post-drying procedure was designed only for laboratory work (i.e. based on work with a glovebox) and the experiments were conducted with single electrode sheets with freely accessible surface. For the industrial post-drying of whole coils the Argon post-drying is not applicable, as this approach is not able to homogeneously reduce the moisture to a sufficient level due to the long diffusion paths in the coils. Hence, for the post-drying of whole coils, higher intensities are needed, which have to be carefully selected to sufficiently reduce the moisture in the coils without damaging the sensitive microstructure of the electrodes.

1.2. Water Uptake of Conventional Cell Components

The level of moisture in the cell components before post-drying depends on environmental conditions during manufacturing, further processing and cell assembly, as well as on those during storage and transport. In addition, the water uptake is greatly influenced by the material system and the structure of the electrodes.^[1,3] In this study, the material system consists of a graphite anode with a carboxymethyl cellulose (CMC)/styrene butadiene rubber (SBR) binder matrix and a NCM622-cathode with polyvinylidene fluoride (PVDF) binder. As separator a highly flexible, porous composite membrane out of polyethylene terephthalate (PET) and ceramic nanoparticles is applied (Freudenberg-separator FS 3011–23).

Previous studies showed that conventional NCM622-cathodes, which normally account for the highest mass in the cell, absorb the least moisture compared to anodes and separators.^[1,16] This effect can be explained by the strong hydrophobicity of the PVDF binder on the one hand and the low specific surface area of NCM-cathodes and their lower

bonding strength of water on the other hand.^[16,30,31] In contrast to cathodes, anodes absorb large amounts of moisture.^[1,3,16] The reason for this is the binder used, CMC, which, despite its low mass fraction, causes by far the highest moisture uptake within the anode due to its hygroscopic behavior. In contrast, graphite, claiming the highest mass fraction of the anode, adsorbs only small amounts of water. The conductive additive carbon black, used both in anode and cathode, induces small moisture uptake, comparable to graphite.^[3] Regarding the separators, the polymer/ceramic separators, as used in this study, show very hygroscopic behavior, which is caused by their open porosity and the coating of inorganic ceramic nanoparticles.^[1,32] However, their mass fraction in the cell is quite low, so in total they introduce only small amounts of water into the cells.^[1]

1.3. Remoistening After Post-Drying and Hysteresis Behavior

In general, post-drying processes use high temperatures and a low dew point atmosphere, resulting in low water activities in the gas phase.^[3] At vacuum post-drying, the latter is achieved by drawing vacuum, often with additional purging cycles with dry inert gas. During post-drying, the water molecules are removed from the porous structures of the cell components. In common LIB manufacturing processes, the cell production then takes place in dry rooms with dew points around -40 to -60°C and temperatures around 20°C (room temperature).^[2] Therefore, when the cell components leave the post-drying process and enter the dry room, the dew point of the surrounding atmosphere usually rises or in the best case remains constant and the temperature of the cell components drops to room temperature. As a consequence, the cell components start to remoisten immediately (assuming that the cell components were post-dried until an equilibrium moisture was reached). This remoistening cannot be inhibited as long as re-diffusion of the moisture into the pores runs fast enough and/or is given enough time.^[3] However, Eser et al.^[3,33] showed that graphite anodes have a hysteresis behavior in their sorption equilibrium. It can be assumed that the other cell components, namely cathode and separator, show a similar behavior. This hysteresis means that, after being post-dried, the cell components typically undergo remoistening, but the sorption equilibrium, and thus the residual moisture, is on a lower level than prior to post-drying (Figure 1). The remoistening occurs due to the increased water activity or relative humidity of the air that surrounds the cell components. This shows the necessity of a well-adjusted post-drying process: the more the moisture can be reduced during post-drying, the lower the ensuing remoistening.

1.4. Heat and Mass Transfer in Porous Structures

In this study, it is investigated whether post-drying procedures can be designed on the basis of fundamental findings attained in experimental studies and combined with theoretical estima-

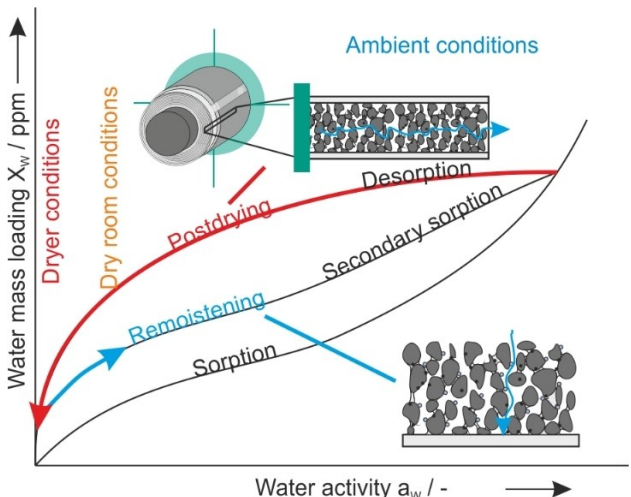


Figure 1. Schematic sketch of the hysteresis behavior of an anode during post-drying and remoistening after post-drying, based on Eser et al.^[33] (reproduced from Ref. [33] with permission, Copyright, 2020, American Chemical Society). Post-drying starts at higher water activities and consequently high water mass loadings. During post-drying, the water activity is reduced and the moisture of the anode is removed. After post-drying, the water activity rises again and remoistening occurs, depending on subsequent processes and environmental conditions.

tions regarding the drying of residual water from electrode coils. In literature, first investigations regarding heat conduction within electrode coils in a vacuum drying process can be found.^[34] The electrode coil consists of a high number of thin layers forming a helical shape: Thin metal layers (e.g. aluminum in case of the cathode) with high heat conductivity and thicker, low conductive electrode layers. In general, the transient heat transport inside the coil can be estimated by the equation for unsteady heat conduction [Equation (1)] using the thermal diffusivity $\kappa = \frac{\lambda}{\rho c_p}$, which depends on the thermal conductivity λ , the heat capacity c_p and the density ρ .

$$\frac{\partial T}{\partial t} = \kappa \nabla^2 T \quad (1)$$

The cylindrical shape of the battery coil appears predestined to describe the heat conduction in a cylindrical coordinate system. Accordingly, the heat conduction is described in the form of Equation (2).

$$\frac{\partial T}{\partial t} = \kappa \left(\frac{\partial^2 T}{\partial r^2} + \frac{1}{r} \frac{\partial T}{\partial r} + \frac{1}{r^2} \frac{\partial^2 T}{\partial \varphi^2} + \frac{\partial^2 T}{\partial z^2} \right) \quad (2)$$

The mass transport of water in an electrode coil is complex. In order to describe it, the mass transport in the gas phase of the porous structure needs to be considered. Due to the large dimensions of the coil in comparison to the thickness of an electrode, a simulation requires a spatially resolved description. Additionally, the mass transport in the materials of the electrode, which is a multi-component system, needs to be considered as soon as water is absorbed into the solid phase of the materials. If the mass transport of water in a coil of an

electrode is to be described, symmetry conditions can be exploited. Water can only leave the coil in axial direction, as the metal foil prevents a radial mass transport, so the relevant diffusion length of the gas phase is half of the electrodes width. This simulation domain is shown in Figure 2.

The consideration of a homogeneously heated, isothermal coil reduces the simulation domain to one section of the electrode coil, which is representative for the mass transport of the whole electrode. In this electrode section, the electrode aims for a sorption equilibrium with the surrounding gas phase. Therefore, an activity adjusts at the phase boundary on the surface of the electrode corresponding to the locally present relative humidity within the porous structure.

The sorption equilibrium at a phase boundary can be described by the equation by Raoult and Dalton [Equation (3)].

$$\tilde{y}_{i,ph} = \frac{p_i}{p} = a_i(\tilde{x}_{i,ph}) \cdot \frac{p_i^*(T_{ph})}{p} \quad (3)$$

In this equation, $\tilde{y}_{i,ph}$ ist the molar fraction of a component i in the gas phase, p_i ist the partial pressure of this component in the gas phase, p is the pressure, a_i is the activity of the component i in the gas phase, $\tilde{x}_{i,ph}$ is the molar fraction at the phase boundary of the solid phase and $p_i^*(T_{ph})$ ist the saturation vapor pressure at the phase boundary. While the correlation of the water activity and the mass loading in the solid phase is recorded in sorption isotherms, the saturation vapor pressure can be calculated with an Antoine equation.

In the post-drying process for LIBs, particularly low activities, and therefore low mass loadings, can be achieved by reducing the partial pressure in the gas phase and by increasing the electrode temperature. The kinetics of mass transport can be influenced by various mass transport

resistances in the gas and the solid phase. Depending on the material system, further assumptions for simplification can be made. Given that neither the binder nor the particles absorb moisture within their volume and the moisture is only adsorbed on the surface of the materials, the limiting mass transfer resistance is caused by the diffusion within the porous structure. The driving force for the mass transport is then the partial pressure gradient between the vapor pressure within the coil and the partial pressure corresponding to the dew point in the vacuum oven. The governing diffusion equation is depicted in Equation (4).

$$(1 - \varepsilon) \rho_s \frac{dX_{W,S}}{dt} + \varepsilon \tilde{M}_w \tilde{\rho}_G \frac{d\tilde{y}_w}{dt} = \frac{\varepsilon}{\tau} \tilde{\rho}_G \tilde{M}_w \frac{d}{dz} \left(D_{W,G} \frac{d\tilde{y}_w}{dz} \right) \quad (4)$$

The quantities annotated with a tilde describe molar-based quantities and the ones without describe mass-based quantities. Epsilon (ε) is the porosity of the electrode, rho (ρ) is the density of either the solid (S) or the gas (G) phase and tau (τ) accounts for the enlarged diffusion path due to the porous structure according to Zehner et al.^[35] \tilde{M}_w is the molecular weight of water. The capitalized letter X stands for the solvent loading of the solid. The lower-case \tilde{y} represents the molar fraction of water in the gas phase. The molar fraction can be converted to solvent loading with the sorption equilibrium and vapor pressure and vice versa. In this equation, $D_{W,G}$ is the diffusion coefficient of water in the gas phase. Under the assumption that the mass transport process takes place in a continuum of the gas phase and not in the range of Knudsen diffusion, the diffusion coefficient is not only a function of the temperature but also a function of the pressure. This depends

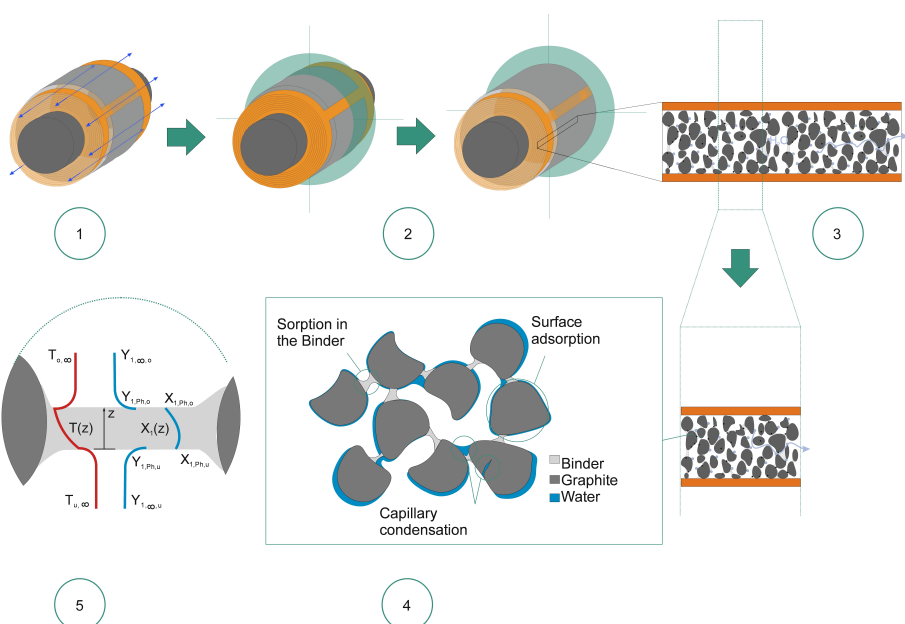


Figure 2. Schematic sketch of the mass transport of water in a (thick) anode coil: (1) axial mass transport, (2) using the symmetry condition, (3) view of a section of an isothermally heated coil, (4) sorption of water in the section, (5) mass transport in the binder.

ence of the diffusion coefficient on the pressure is an argument for reasonable post-drying times in a vacuum process despite long diffusion paths compared to an atmospheric roll-to-roll process. The diffusion coefficient of binary gases can be calculated by the kinetic theory of gases or the Fuller equation.^[36]

The solution of the diffusion equation requires an initial condition [Equation (5)], as well as boundary conditions. Reasonable boundary conditions for an estimation of the drying process are given in Equations (6) and (7).

$$\tilde{y}_W = \frac{p_w^*(T_{D,0})}{p_0} \quad (5)$$

$$\frac{d\tilde{y}_W}{dz}|_{z=0} = 0 \quad (6)$$

$$\tilde{y}_W|_{z=b/2} = \frac{p_w^*(T_D)}{p} \quad (7)$$

The conditions are given for the molar fraction of the gas phase and converted to solvent loading as previously described. The initial condition consists of the initial dew point $T_{D,0}$ and the pressure p_0 . By contrast, the boundary condition in the vacuum oven consists of the dew point and the pressure within the oven. If no purge gas is used, moisture can accumulate in the vacuum oven during the drying process and, thus, increase the dew point or reduce the partial pressure gradient, respectively. This happens due to the fact that gas molecules are removed by the vacuum pump in equal proportions while the electrode coil is a source for further water molecules and, thus, increases their proportion.

1.5. Aim of this Study

This study aims at designing an efficient, well-adjusted and application-oriented vacuum post-drying procedure for electrode coils. Based on previous fundamental findings attained in experimental studies, research and theoretical estimations regarding the coil heating and the drying of water from an electrode coil, the possible parameters for post-drying of LIBs were narrowed down. Perceptions of previous experimental findings and research were used to select a post-drying temperature. For the design of the process timing, theoretical estimations concerning the heat transfer in the coils were made for anode and cathode. The estimations regarding the mass transfer were only conducted on the basis of the cathode. The reason for this is that the mass transport in the anode is very difficult to estimate due to the solid material diffusion in the most commonly used binder CMC and no literature concerning the diffusion processes in anodes exists. After having designed the post-drying procedure, it was experimentally applied on the basis of coils with different electrode lengths and coating widths.

2. Results and Discussion

2.1. Design of a Post-Drying Procedure

As mentioned above, there is still a lack of research concerning the post-drying step and its influence on structural and electrochemical properties of LIBs.^[21] However, some studies have shown that higher post-drying temperatures/intensities can have a strong negative impact.^[1,27] In addition, several studies exist where good cell performance is achieved by moderate post-drying temperatures and/or hold times.^[22–24,28] The crucial factor for post-drying whole electrode coils is to enable diffusion through the half of the coating width to a sufficient scale, so the major challenge lies within the long diffusion paths compared to post-drying of sheets with freely accessible surfaces. Diffusion can be accelerated by high temperatures, low vacuum and a high concentration gradient, so low dew points in the vacuum oven. As the temperature seems to be a limiting factor when post-drying LIB electrodes, the temperature was set to a moderate, safe level of 80 °C on the basis of experimental findings and research.^[1,22–24,27,28] Then, heat transfer estimations were made for cathode and anode to determine the necessary pre-heating time to reach 80 °C in the whole coils (cf. Heat Transfer Estimations in the Experimental Section). On the basis of the estimations, the pre-heating phase (phase I) was set to 2 hours. As heat transfer in the gas phase is impeded by vacuum, the decision was taken to conduct pre-heating at atmospheric pressure (1 bar). After that, phase II of the post-drying procedure, the actual post-drying phase, was designed. In this part, purging cycles with a dry gas play a very important role. First of all, one has to keep in mind that there is no total vacuum in the oven. Typical total pressures in vacuum post-drying are in the range of 10 mbar. Thus, at the beginning of the post-drying process, 10 mbar of air or Argon are in the oven and now the moisture is released from the electrode or separatore coils into the oven during post-drying. The concentration of moisture in the oven rises and the dew point increases towards worse values. If the wet gas phase in the oven is not removed, it cannot absorb more moisture from the coils. Thus, the moisture cannot be further reduced and an equilibrium between wet coating and wet gas phase in the oven is established. While the vacuum pump pulls constantly out the gas phase of the oven, it removes not only the water molecules, but also the dry gas molecules. If no dry gas is added, the dew point within the vacuum oven will constantly rise, until finally almost all gas molecules in the oven are water and no further post-drying of the electrode is possible. By Argon purging, dry Argon is pulled into the oven and the equilibrium between water molecules and dry Argon is moved to lower water concentrations and hence lower dew points. Now, there is again a concentration gradient between the coating of the electrode and the Argon in the oven and more moisture can be released. By this, a very high moisture reduction can be achieved. The purging cycles in this study were laid out pursuant to the speed and final vacuum of the vacuum oven and set to an amplitude from 10 mbar to 30 mbar with a hold time of 10 min at 10 mbar at each time.

The necessary hold time of phase II was then estimated with the preassigned conditions on the basis of mass transfer in a cathode coil and set to 4.7 hours (cf. Mass Transfer Estimations in the Experimental Section). Altogether, a II-phase vacuum post-drying procedure containing a heating phase (80°C /2 h/atmospheric pressure) and a vacuum post-drying phase (80°C /4.7 h/14 purge cycles between 10 and 30 mbar) was designed (Figure 3). Note that the specific calculations and the newly designed post-drying procedure are namely applicable to LIB electrodes with differing compositions, divergent conductive agents or varying manufacturers of the materials, but not to binder systems divergent from those of this study, as the sensitivity towards higher post-drying intensities, the moisture uptake and release as well as the post-drying behavior are strongly dependent on the chosen binder system. However, in principal the simulation model is applicable to other binders if the appropriate material parameters are used.

2.2. Residual Moisture Content

For the applicability of the post-drying procedure for wider coating widths and/or larger coils, two factors are crucial: Firstly, the duration of the heating phase (phase I) must be set long enough to guarantee a homogeneous temperature in the whole coil. Secondly, the amplitude and the frequency of the purging cycles of the post-drying phase (phase II) have to be high enough to enable uptake and removal of the released moisture, even at higher amounts.

In the following, the results of the Karl Fischer Titration measurements are presented. With regard to the moisture content in the post-dried state, it always has to be considered that this state is already the remoistened state. As remoistening

occurs immediately after the end of the post-drying process and very fast^[3], it is not possible to take samples or to assemble the cells before the cell components remoisten. This is why, after post-drying, all samples were exposed in the dry room for 1 hour before being measured, to guarantee an equilibrium with the surrounding atmosphere.

2.2.1. Coating Width

In order to prove that the designed post-drying procedure is also applicable for wider coatings, electrode coils with coating widths of 11 cm and 24 cm (electrode length within coils $M = 10\text{ m}$) were post-dried (Vacuum post-dried = Vac.-PD) and compared with respect to their residual moisture (Figure 4). In general, very high moisture reductions were attained for both electrodes: The average moisture reduction amounted to 88% for the cathode and to 70% for the anode. Compared to the cathodes, the anodes contained high amounts of moisture both before and after post-drying, which can be explained by the usage of the hygroscopic binder CMC and the aqueous processing of the anode slurry.^[1,3,16] The moisture enclosed in the CMC is difficult to remove by post-drying, and the hygroscopic binder causes high remoistening after post-drying. Moreover, it can be observed that the moisture contents of the non-post-dried (non-PD) anodes varied significantly (11 cm vs. 24 cm). As the anodes were manufactured in several dissolver batches on different days, according to the experimental section, this can be attributed to the influence of different ambient conditions during dispersion, coating and drying. In addition, the hygroscopic binder, CMC, massively absorbs moisture of the surrounding atmosphere and hence is very sensitive to fluctuating dew points.^[1,3]

With regard to the coating width, the electrodes with a broader coating width had 2.18 times (24 cm/11 cm) more coating weight and a higher amount of absolute water before

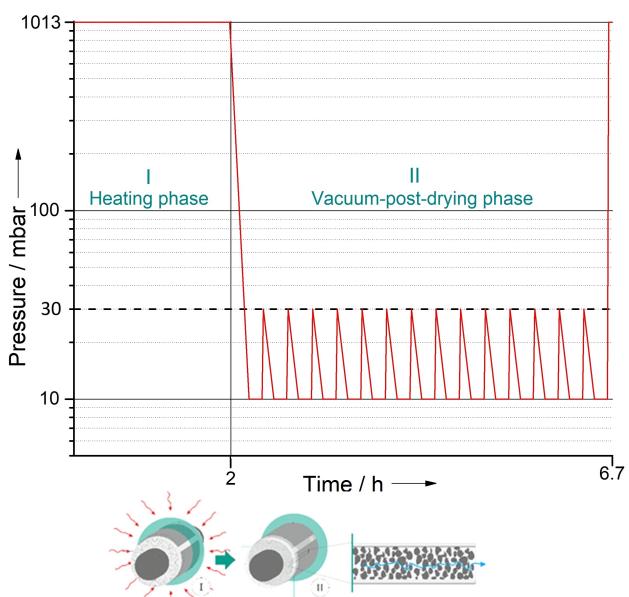


Figure 3. Presentation of the designed procedure for post-drying of electrode and separator coils in vacuum ovens with a schematic sketch of the two post-drying phases by the example of a cathode coil.

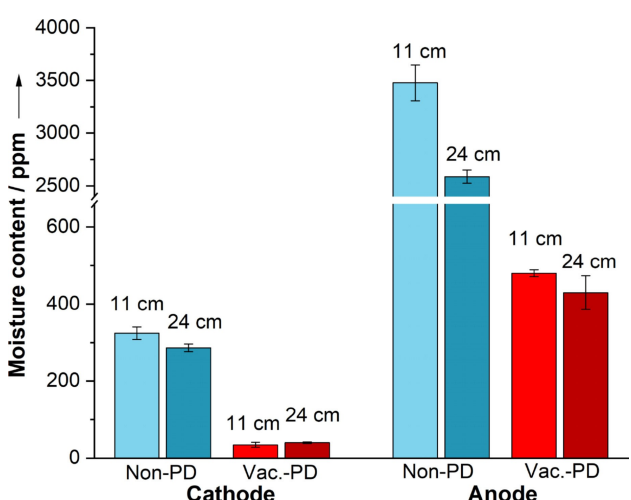


Figure 4. Comparison of moisture contents before (Non-PD, normal atmosphere) and after vacuum post-drying (Vac.-PD, dry room) for anodes and cathodes with a varying coating width. Electrode length within coil: 10 m (M).

post-drying respectively, since the mass loading remained the same. By post-drying, the moisture of the anode was significantly reduced to 480 ppm (11 cm coating width) and 430 ppm (24 cm coating width), so the wider anode even reached a lower ppm-moisture. The relatively small difference in residual moisture between both anodes was most likely caused by different dew points during 1 hour remoistening. Regarding the cathodes, very low and almost identical residual moisture contents of 34 ppm (11 cm coating width) and 40 ppm (24 cm coating width) were attained. Summarizing, the results prove that the chosen post-drying parameters enable adequate axial diffusion even for the wider electrode coatings up to 24 cm and a sufficient take away of the released moisture. Moreover, the results show that a further reduction of the already short process time would be possible for the 11 cm wide electrodes.

Figure 5 shows the calculated post-drying curves for the two different coil geometries with a width of 11 cm and 24 cm in comparison to the experimental data of the cathode. This comparison clarifies the time points within the post-drying curve at which the experimental data was acquired. The initial values deviate slightly from the initial value of the theoretically estimated post-drying curve due to previously discussed reasons, as well as a lack of perfectly adjusted sorption equilibrium of the sample's components. During the heating period, already up to 40% of the initial moisture content is removed from the coil sample. The initiation of the vacuum period results in a new boundary condition for the post-drying process and accelerates the mass transport through the electrode. The steep slope at the beginning of the vacuum period shows the accelerated mass transport due to the pressure decrease, as well as the decrease in partial pressure of water. The fluctuations in the drying curve succeeding this

transport acceleration occur because the diffusion is sensitive to the pressure change during the purging cycles. The diffusion path, i.e. the width of the electrodes, has a quadratic effect on the post-drying time.

The post-drying process is terminated after 6.7 hours and the resorption in the dry room begins. As mentioned above, obtaining experimental data immediately after the termination of the post-drying process is not possible with the current experimental setup, and small deviations in the immediate sample preparation time will cause significant moisture content changes. Therefore, only the samples resorbed at dry room conditions can be compared to the simulation. During this resorption, the coil is unwound, which results in short diffusion paths and a rapid adjustment of the equilibrium water content. The heat transfer for a single electrode sheet is also significantly accelerated compared to an electrode coil. Thus, the resorption at dry room conditions is estimated with an electrode sheet at dry room temperature. The water activity is the crucial factor during resorption, as it determines the equilibrium moisture content at a given environment. As pointed out in Equation 3, this water activity is the vapor pressure in the gas phase at dew point temperature divided by the vapor pressure at electrode temperature. Thus, the combination of the dew point temperature and the electrode temperature determines the amount of water that is desorbed by the electrode in the oven as noted in Equation (8).

$$a_{W,Oven} = \frac{p_w^*(T_{D,Oven} = -80^\circ\text{C})}{p_w^*(T_{E,Oven} = 80^\circ\text{C})} = \frac{0.000534 \text{ mbar}}{472.71 \text{ mbar}} = 1.1 \cdot 10^{-6} \quad (8)$$

Comparing the water activity in a vacuum oven at $T_{Oven} = 80^\circ\text{C}$ and $T_{D,Oven} = -80^\circ\text{C}$ to the water activity at dry room conditions further justifies this estimation with regard to its final equilibrium state. The water activity in the vacuum oven ($a_{W,Oven} = 1.1 \cdot 10^{-6}$) is orders of magnitudes lower compared to the dry room water activity ($a_{W,Dry\ room} = 2.6 \cdot 10^{-3}$, $T_{D,Dry\ room} = -45^\circ\text{C}$, $T_{E,Dry\ room} = 23^\circ\text{C}$). Consequently, the electrode resorbs moisture when being transferred from the vacuum oven to the dry room, due to the higher dew point and the lower temperature, which both increase the water activity. As for a single electrode sheet the heat and mass transport resistances are low, the equilibrium state with dry-room conditions will be reached within minutes after unwinding the coils. The estimated values from the simulation match the experimental data of the 24 cm coil very well. However, the estimated post-drying curve of the 11 cm wide coil overestimates the experimental data. A possible explanation are inevitable local fluctuations of the dry room conditions at the time of moisture determination. The experimental data points are in close proximity, which indicates that both coils reached similar moisture contents at the end of the vacuum process and therefore resorbed moisture accordingly. For a thorough validation of the simulation, time resolved moisture levels of the coils need to be tracked. However, the simulation indicates the moisture level propagation inside the

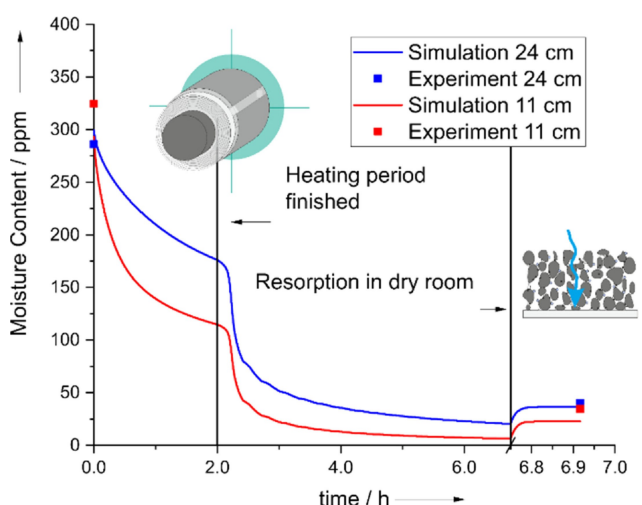


Figure 5. Estimated drying curves (lines) and experimental results (squares) of the cathode coil. The simulation considers a dew point of -80°C in the oven. The termination of the heating period induces a pressure decrease from 1 bar to 0.01 bar and the vacuum phase includes the purging cycles according to the experimental procedure. The remoistening succeeding the drying procedure is considered to the dry room dewpoint of -45°C . The graphical icons indicate the simulation domain and the considered diffusion paths.

electrode coil over time as well as the influence of the varying coil lengths, which adds to a fundamental understanding of the drying process.

2.2.2. Coating Length

In order to investigate if the designed post-drying procedure is also applicable for longer lengths and, thus, coil diameters, three different electrode lengths ($S=5\text{ m}$, $M=10\text{ m}$, $L=20\text{ m}$) were investigated (Figure 6). As the diffusion length is not a function of the electrode length and resulting coil diameter but only of the coating width, the only crucial factors for the application for longer lengths are to achieve a homogenous heating in phase I and a sufficient removal of the higher amounts of released moisture by the purge cycles in phase II. As the results show, no influence of the electrode length on the residual moisture content is identifiable after post-drying, which proves that the designed post-drying procedure is also applicable for longer electrode lengths. Again, the cathodes achieved a very low, almost identical moisture content after post-drying. On the contrary, the anodes show significantly higher moisture contents after post-drying, which again can be traced back to their hygroscopic behavior and higher remoistening. In addition, after post-drying, the moisture contents of the anodes (S - vs. M - vs. L -length) vary more than those of the cathodes. This observation underlines the high influence of remoistening caused by higher dew points, which should especially not be underestimated in the case of the anode. Nevertheless, the results show that the designed post-drying procedure enables the adequate post-drying of anodes and cathodes with lengths that differ by the factor 4 ($S=5\text{ m}$ vs. $L=20\text{ m}$) to low residual moistures.

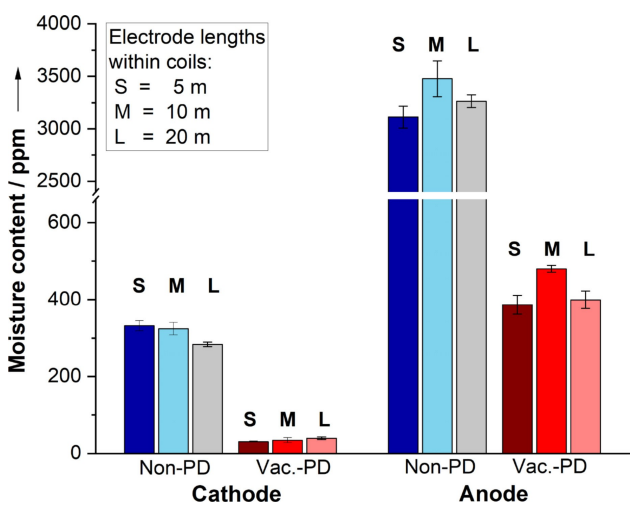


Figure 6. Comparison of moisture contents before (Non-PD, normal atmosphere) and after post-drying (Vac.-PD, dry room) of anode and cathode with varying lengths within the coils. Coating width: 11 cm.

2.3. Hysteresis Behavior

As mentioned above, after post-drying, remoistening of the cell components to a certain degree is inevitable. Nonetheless, Eser et al.^[3,33] showed that the anodes demonstrate a hysteresis behavior. Due to this hysteresis behavior, remoistening of the anode after post-drying occurs, but to a lesser extent than prior to the post-drying process (Non-PD state) (Figure 1). A similar hysteresis behavior for the cathode and separator can be assumed, but has not been proven yet. Therefore, a coil of the Freudenberg separator with 10 m length (M-coil) was post-dried with the designed post-drying procedure as well. Although the Freudenberg separator is more heat-resistant than the electrodes, and higher post-drying intensities are suggested by the manufacturer, in this study the separator was post-dried with the same procedure as the electrodes to enable a direct comparison between the moisture reduction achievements. Afterwards, hysteresis experiments of anode, cathode and separator were carried out with sheets of the Vac.-PD M-coils by exposing them to normal atmosphere for 18 hours.

The results were in accordance with Eser et al.^[3,33], and demonstrated that not only for the anode, but also for the separator and the cathode, the remoistened state (remoistened=rem.) was lower than the Non-PD state (Figure 7). However, the moisture content difference before post-drying and after remoistening at normal atmosphere was not large, as the remoistening dew point was comparatively high. These observations highlight two important factors for a successful post-drying result and a low residual moisture during cell assembly: Firstly, the moisture reduction by post-drying should be as high as possible, without damaging the electrode structure, to reach a low sorption isotherm. Secondly, further processing after post-drying should take place in dry rooms with low dew points to maintain a low moisture level.

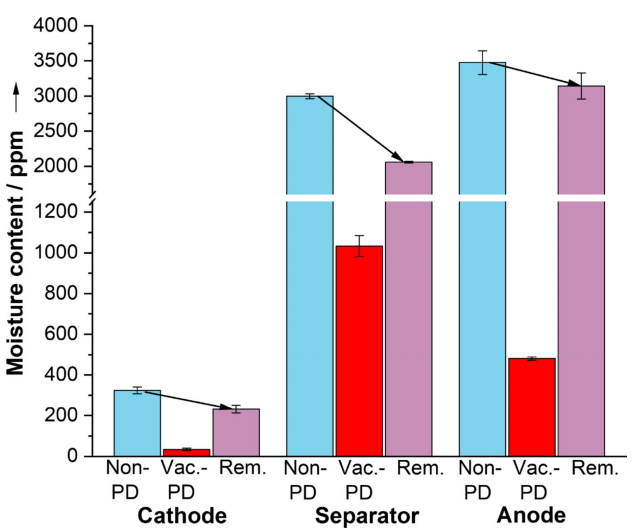


Figure 7. Hysteresis behavior of cathode, separator and anode demonstrated by the moisture contents before (Non-PD, normal atmosphere) and after post-drying (Vac.-PD, dry room) as well as after remoistening (remoistening=rem., normal atmosphere). Electrode/separator length within coil: 10 m (M), coating width of electrodes: 11 cm.

2.4. Cell Assembly - Residual Moisture and Physical and Electrochemical Properties

The electrochemical C-rate capability and long-term performance of the vacuum post-dried coils were tested in single-compartment pouch cells. As mentioned above, it was shown in a previous study that high post-drying intensities can lead to the deterioration of the electrochemical performance.^[1] A very mild post-drying procedure, referred to as Argon-PD, consisting of three cycles of Argon purging and vacuum drawing at 20°C in the lock of an Argon-glovebox, was identified as the best procedure. It should be noted that only sheets of electrodes and separators with freely accessible surfaces and extremely short diffusion paths were post-dried in the previous experiments, so this procedure is only applicable for laboratory work.^[1] For post-drying of coils with inaccessible surfaces, this post-drying procedure is not suitable, as the diffusion paths are quite long in coils. However, as this post-drying procedure showed the best results compared to other vacuum-post-drying procedures (e.g. 18 hours at 120 °C^[1]), it was taken as reference post-drying procedure in this study. Therefore, sheets of the Non-PD coils were taken, post-dried with Argon-PD and assembled under the same conditions as the Vac.-PD cells. It is important to note that remoistening after Argon-PD did not occur since the samples were directly transported from the lock into the Argon-glovebox for cell assembly.

2.4.1. Residual Moisture After Cell Assembly

In Figure 8, the moisture contents of samples taken during cell assembly in the Argon-glovebox are displayed and compared to the Non-PD state. While in the case of the anodes the higher moisture level can be explained by the CMC binder, in the case

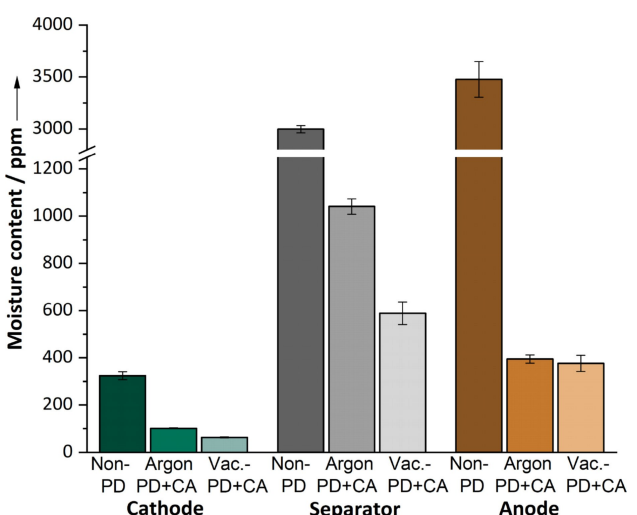


Figure 8. Comparison of moisture of the non-post-dried state (Non-PD, normal atmosphere) with Argon post-dried (Argon-PD, single sheets) and Vacuum post-dried (Vac.-PD) samples of electrodes and separator taken during cell assembly (CA, Argon atmosphere). Argon-PD: single sheets, Vac.-PD: electrode/separator length within coil = 10 m (M), coating width of electrodes = 11 cm.

of the separators the high water uptake is caused by the open porosity and coating of inorganic ceramic nanoparticles.^[1,3,32] Compared to the state after post-drying and 1 hour exposition in the dry room (cf. Figure 7), the Vac.-PD cathode contained more moisture after cell assembly, whereas the moisture of the Vac.-PD separator and anode was further reduced (cathode: 63 ppm, separator: 588 ppm, anode: 376 ppm). On the one hand, the cathode could have been remoistened during the handling and cell preparation in the dry room, as the dew point fluctuates during the day due to differing occupancy and other experiments. On the other hand, the cathode could have absorbed some moisture from the other cell components in the packaging or during cell assembly. On the contrary, the further moisture reduction of separator and anode can be explained by the fact that high remoistening occurred during exposition in the dry room after post-drying due to their hygroscopic properties. When exposed to the dry Argon-air in the glovebox for test cell assembly with a quite lower dew point than in the dry room, a high amount of the remoistening-moisture could be easily removed again so that a lower moisture level was attained.

The comparison of the moisture reduction of both post-drying procedures and cell assembly under Argon atmosphere shows that both procedures are able to significantly reduce the residual moisture of all cell components although Argon-PD (20°C/15 min/3 Vacuum-Argon purging cycles) has a considerably lower post-drying temperature and duration than Vac.-PD (80°C/6.7 h/various Vacuum-Argon purging cycles, cf. Table 1). Among other things, this can be explained by the fact that the Argon-PD procedure was conducted on punched-out electrode samples with freely accessible surfaces, so very short diffusion paths, and a significantly lower final vacuum than Vac.-PD ($p_{final}(\text{Argon-PD}) < 0.01 \text{ mbar}$, $p_{final}(\text{Vac.-PD}) = 10 \text{ mbar}$), which further accelerates diffusion. However, above all, no remoistening occurred to the samples after Argon-PD as they were directly transferred into an Argon-glovebox for test cell assembly afterwards, which especially has a high impact on the residual moisture of the hygroscopic cell components separator and anode. However, the Vac.-PD samples still reached a lower residual moisture for all three cell components during cell assembly under Argon atmosphere despite their preceding remoistening. Altogether, the results demonstrate the good

Table 1. Parameters and hold times of the designed post-drying procedure. The temperature was set to 80 °C.

Phase	Step	Cycles	Start pressure [mbar]	Final pressure [mbar]	Step time [min]
I	1. Heating	1013	1013	1013	120
II	1. Pressure reduction	1013	10	10	15
	2. Hold time	10	10	10	10
	3. Purging Cycles	14			
	Purging	10	30	30	0,5
	Drawing vacuum	30	10	10	7,5
	Holding vacuum	10	10	10	10
	5. Ventilating	10	1013	1013	3

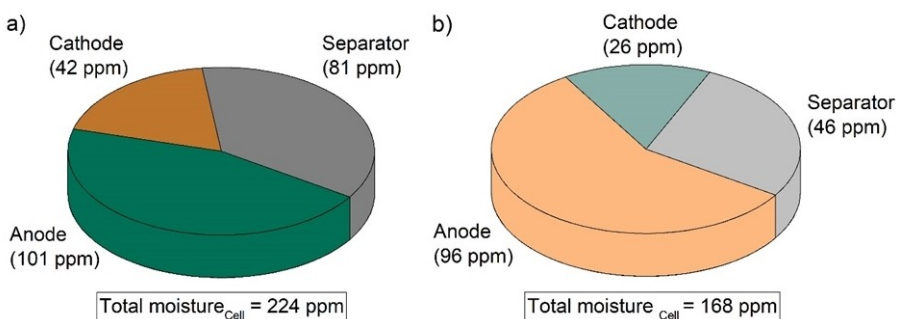


Figure 9. Total moisture of the single compartment pouch cells built with components post-dried with a) the Argon-PD and b) the designed Vac.-PD procedure. Calculation according to the mass ratios of cathode, anode and separator in the cell without electrolyte and housing.

applicability of the designed Vac.-PD procedure for the post-drying of whole coils.

Significant differences in the post-drying results can be observed, especially for the cathodes (Argon-PD: 101 ppm, Vac.-PD: 63 ppm) and the separators (Argon-PD: 1040 ppm, Vac.-PD: 588 ppm). However, concerning the anode there is only a slight difference in residual moisture (Argon-PD: 394 ppm, Vac.-PD: 376 ppm). This can be attributed to the fact that anodes remoisten to a great extent, even at the low dew points of dry rooms, due to the hygroscopic CMC binder.^[3] Hence, if remoistening had been prevented after Vac.-PD as well, the difference between Argon-PD and Vac.-PD would have been higher since Vac.-PD is able to reduce the residual moisture to a higher degree, due to its higher intensity.

In Figure 9, the total cell moisture, as well as the moisture which was introduced by the single cell components according to their mass ratio, is displayed for Argon-PD and Vac.-PD. The total cell moisture was calculated with regard to the mass ratios of cathode, separator and anode in the cell (50% cathode, 8% separator, 42% anode, current collectors included) and without electrolyte or housing. Despite claiming a lower mass ratio than the cathode, the anode introduced the highest amounts of moisture into the cells after both post-drying procedures, due to its much higher residual moisture after post-drying. Both post-drying procedures led to very low total cell moisture amounts of 224 ppm after Argon-PD and 168 ppm after Vac.-PD. By Vac.-PD, a higher moisture reduction was achieved despite remoistening, which again proves the good adjustment of this post-drying procedure. It also has to be considered that the difference in total moisture is not distributed equally: whereas the anode is only 4.95% drier after Vac.-PD compared to Argon-PD, the cathode contains 38.1% and the separator even 43.21% less moisture.

2.4.2. Specific Electrical Resistance after Cell Assembly

In previous studies it was observed that moisture reduction achieved by mild post-drying can reduce the specific electrical resistance of both cathode and anode.^[1] However, very high post-drying intensities (120 °C/vacuum/96 h) damaged the polymeric 3D networks and their electrical percolation path-

ways for both anode and cathode. This dramatically increased the specific electrical resistance that, in turn, led to a deterioration of the electrochemical performance.^[1] Therefore, measurement of the specific electrical resistance allows conclusions concerning possible changes or damage of the polymeric 3D networks by the post-drying procedures. In Figure 10, the specific electrical resistances of anodes and cathodes after post-drying with Argon-PD or rather Vac.-PD and cell assembly in Argon-atmosphere are shown, and compared to the Non-PD state.

For the cathode, the moisture reduction achieved by Vacuum post-drying led to a significant decrease of the specific electrical resistance. That moisture reduction obtained by gentle post-drying can reduce the resulting specific electrical resistance is in accordance with previous studies, and proves that the polymeric 3D network was not impaired by Vacuum post-drying.^[1] Moisture seems to constitute an obstacle within the conductive agent/binder matrix that interrupts electrical percolation pathways. However, after Argon-PD, the specific

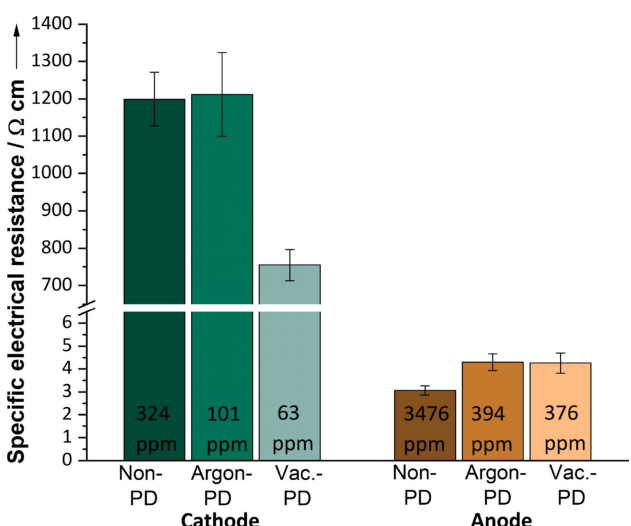


Figure 10. Comparison of the specific electrical resistances of cathode and anode samples taken before (Non-PD, normal atmosphere) and after post-drying (Argon-PD and Vac.-PD) during cell assembly in Argon-atmosphere. Argon-PD: single sheets, Vac.-PD: electrode length within coil = 10 m (M), coating width = 11 cm.

electrical resistance was not reduced compared to Non-PD in this study, although the standard deviation was quite high. This could indicate that by Argon-PD, a more inhomogeneous moisture reduction occurs, leading to parts with lower residual moisture and lower specific electrical resistance and parts with higher. Above all, the observations show that despite its high moisture reduction capability, the designed Vac.-PD method is still gentle enough to avoid damaging the polymeric 3D network of the cathode. Comparing the results of Argon-PD and Vac.-PD, it may be supposed that not only the moisture reduction, but the combination with higher temperatures of 80 °C, leads to a high decrease of the specific electrical resistance of cathodes. The PVDF binder of the cathodes is a thermoplastic, which starts creeping at specific high temperatures and under continuous load.^[1,37] Thus, one possible explanation could be that after moisture removal, the thermoplastic 3D network is able to rearrange to a certain degree and to bridge voids within the network, due to thermally activated diffusion creeping and the pulling effect of the vacuum. As the specific electrical resistance of the cathodes decreased after Vac.-PD, the rearrangements that occurred were most likely small enough to not damage the electrical percolation pathways. Altogether, the newly established Vac.-PD procedure lead to a significant decrease of the specific resistance of 37% for the cathode.

In comparison, the anode showed very low specific electrical resistances in general. Nevertheless, the specific electrical resistance was slightly increased by both post-drying procedures. This can be explained by the shrinkage behavior of CMC during water removal, which leads to a shrinkage of the whole 3D CMC/SBR binder matrix and the loss of surface contacts.^[1,38,39] As after both post-drying procedures the specific

electrical resistance was more or less the same, the results show that the designed Vac.-PD procedure is gentle enough to not impair the conductive agent/binder-matrix of the anode any more than the mild Argon-PD procedure. In previous studies, the removal of moisture by mild post-drying led to a slight decrease of the specific electrical resistance.^[1] However, in that study the anodes were not calendered, which is why there was a higher porosity and less tension in the coating.

2.4.3. Electrochemical Performance

The electrochemical long-term performance and the C-rate capability of the one-compartment pouch cells subjected to different post-drying procedures are shown in Figure 11. The cell capacity was normalized to the mass of the cathode material, NCM622, as the lithium ions in LIBs are mainly provided by the active material of the cathode, which consequently is a limiting factor for the cell capacity.^[1] Furthermore, normalization of the cell capacity with respect to the active material on the cathode's side allows a direct comparison with the data of manufacturers or other scientific studies.

Although no differences can be observed during formation, already in the first C-rate test at 1 C, the Argon-PD cells were seen to perform worse than the Vac.-PD cells. During further C-rate testing and long-term cycling, the Argon-PD cells showed a distinct decline and a higher standard deviation. On the contrary, the Vac.-PD cells performed better during all C-rate tests and demonstrated highly stable long-term cycling. The Argon-PD cells could only reach the same discharge capacities as the Vac.-PD cells during recovery at 0.1 C.

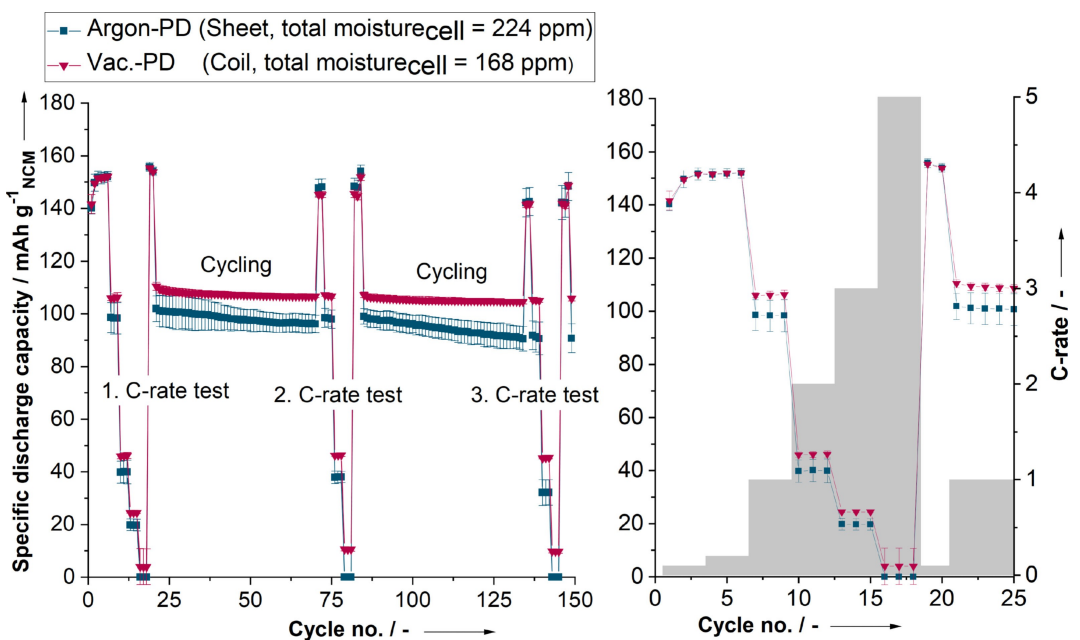


Figure 11. Specific discharge capacities of one-compartment pouch cells resulting from the two compared post-drying procedures (Argon-PD and Vac.-PD). Left: presentation of 150 cycles containing 3 C-rate tests and 2 cycling phases. Right: Detailed presentation of the first 25 cycles with indication of the respective C-rate. Average of 3 cells each.

However, even the Vac.-PD cells did not reach specific capacities as high as reported in literature.^[40] This has several reasons: Firstly, the used Freudenberg-separator was primary designed with regard to a high safety^[41], whereas the cell performance was secondary. Secondly, relatively thick electrodes with high mass loadings of 27.1 mg cm^{-2} for the cathode and 13.73 mg cm^{-2} for the anode, which corresponds to a total cell capacity of 4.6 mAh cm^{-2} , were produced for this study in order to measure and to identify the influence of the post-drying procedures on residual moisture. Unfortunately, thicker electrodes suffer from limited ionic and electronic transfer at elevated C-rates, which impairs their electrochemical performance.^[42,43] Another reason for an increaseable capacity especially at higher C-rates is the low content of carbon black (1.5 wt%) and graphite (0.75 wt%) in the cathode. In literature, higher amounts of conductive additives are used to reach higher discharge capacities, however, this was not the aim of the present study as the chosen electrode compositions were industry-oriented.^[1,29,44] Another reason for the increaseable discharge capacities during cycling can be found in the preceding C-rate test which was conducted up to 5 C even with these thick electrodes to generate clear differences between both post-drying procedures. High C-rates can lead to irreparable capacity fading due to the loss of primary and secondary active material as well as rate capability losses.^[45]

Furthermore, the Argon-PD cells of this study showed a worse performance than cells post-dried equally in a previous study.^[1] Two reasons can be identified for that: Firstly, different electrodes with other mass loadings and balancing were used and the anodes of this study were calendered in contrast to those of the previous study. Due to the calendering, the ion diffusion could have been hindered, especially at higher C-rates. Secondly, in the current study another separator, namely Freudenberg, was used, whereas Separion was applied in the previous study. Because of differences concerning material composition, thickness and porosity, it is highly probable that the separators react in a different way to the applied post-drying procedures and to different residual moisture levels in the cells. Additionally, as mentioned above, the Freudenberg separator used in the current study was designed with regard to safety.^[41] Note that a direct comparison of the moisture reduction achieved in both studies is not possible, as in the previous study the moisture was calculated including the weight of the current collectors, whereas in the present study it was determined without the weight of the current collectors, as they only absorb marginal amounts of moisture.^[1,16]

With regard to the electrochemical results of this study, the data shows that the designed Vac.-PD procedure is able to sufficiently reduce the moisture of the cell components without damaging the sensitive conductive agent/binder-matrix of the electrodes. An explanation for the better performance of the Vac.-PD cells than the Argon-PD cells at higher C-rates can be found in the significantly lower specific electrical resistance of the cathode (Figure 10). Another probable reason is the lower residual moisture of the cell components and, consequently, the assembled cells (Figure 8 and Figure 9) after Vac.-PD. However, it is very likely that it is especially the moisture

distribution within the cell which has a strong influence on the cell performance. As explained in chapter 2.4.1, the moistures in the different cell components (anode, separator, cathode) are not similarly lower in case of Vac.-PD compared to the case of Argon-PD. Instead, the anode has only 4.95% less moisture after Vac.-PD compared to Argon-PD whereas the cathode contains 38.1% and the separator even 43.21% less moisture. Taking into account the lower specific electrical resistance of the cathode after Vac.-PD, the results indicate that very likely not only a lower moisture level, but in particular the moisture distribution in the cells has a strong impact on the cell performance.

In order to further investigate the reason for the different C-rate capabilities of the differently post-dried cells, the specific differential capacity vs. voltage profiles were determined from the charge and discharge curves of the best cell from each post-drying procedure (Figure 12). For this, the capacities of cycles no. 2, 5 and 8 were analyzed, corresponding to C-rates of 0.1 C/0.1 C (charge/discharge), 0.2 C/0.2 C and 0.2 C/1 C, respectively. In the curves, two redox peaks between 3.5 V and 3.8 V during charging and between 4.1 V and 3.5 V during discharging can be detected, which is characteristic for NCM622 vs. graphite anodes.^[46–48] The first redox peak in the charge curve indicates the removal of the lithium ions from the NCM-cathode and their intercalation into the graphite anode ($\text{C}_6 \rightarrow \text{LiC}_6$), and the second peak results from phase transitions of NCM.^[46–48] In the discharge curve, the peaks correspond to the respective reverse reactions. In literature, different information concerning the phase transition at the second peak in the charge curve exist: Noh et al.^[46] and Jung et al.^[47] explained the second peak by a phase transition from a hexagonal (H) to a monoclinic (M) lattice of NCM ($\text{H} \rightarrow \text{M}$). However, this explanation was derived from studies about the phase transitions of pure LiNiO_2 .^[49,50] Zheng et al.^[50] studied the

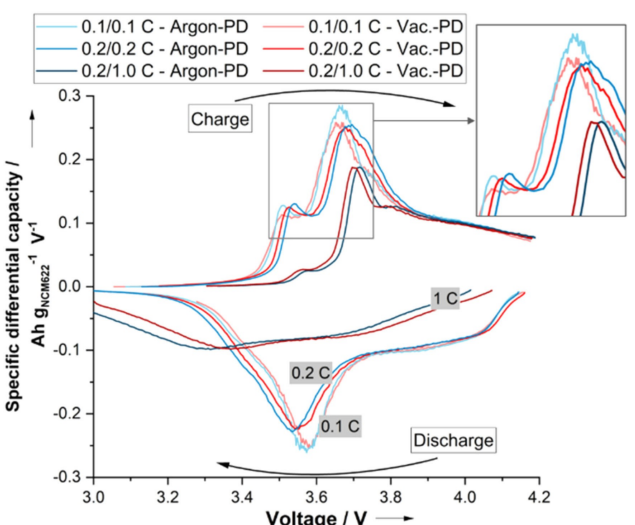


Figure 12. Specific differential charge and discharge capacities vs. voltage curves (smoothed by a moving average) of the best running cell of each post-drying procedure at 0.1 C/0.1 C (charge/discharge), 0.2 C/0.2 C and 0.2 C/1 C (\cong cycle no. 2, 5 and 8) in the voltage range of 3.0–4.2 V. Detailed presentation of the charge curve in the voltage range of 3.45–3.75 V.

structural changes in Ni-rich layered materials during charge and discharge via X-ray diffraction and ^{6}Li solid state nuclear magnetic resonance experiments. They found out that the pristine structure of NCM622 is hexagonal (H1) and converts to a Li_M -less ($\text{Li}_M = \text{Li}$ which is predominantly surrounded by Mn^{4+}) hexagonal form (H2) at higher voltages.

Nevertheless, by comparing the differential charge and discharge curves at increasing C-rates, a shift to higher voltages during charging, a shift to lower voltages during discharging and a flattening of the anodic peaks can be observed. This indicates an increasing capacity fade with rising C-rate for both post-drying procedures. At higher C-rates, the charging curve shifts to higher voltages and reaches the upper termination voltage earlier, which is why the cell cannot be charged completely. In addition, due to the higher voltages, more electrical energy is consumed during charging. The discharging curve shifts to lower voltages and reaches the lower termination voltage before the cells can be completely discharged at 1 C. As a consequence, the energy which can be drawn from the LIB decreases.

Comparing Argon-PD with the Vac.-PD in detail, it can be observed that the curves are more or less superimposed at 0.1 C. However, with rising C-rate, the shift of the Argon-PD cell to higher voltages during charging and lower voltages during discharging becomes significantly more pronounced than the shift of the Vac.-PD cell. This explains why the specific discharge capacities of both post-drying procedures were almost the same during formation and recovery but differed crucially during C-rate tests and cycling (Figure 10). The increase in overpotential for the Argon-PD cells is likely due to the production of HF from the higher residual moisture of separator and anode (cf. Figure 9) and the associated impairment of the SEI, leading to accelerated cell degradation and capacity fading.^[1] In addition, the higher specific electrical resistance of the Argon-PD cathode could have led to the shift to higher voltages during charging (or lower voltages during discharging, respectively) due to ion and electron transport limitations. However, further study is required to better understand the influence of different moisture distribution within the cells and different total cell moisture on the electrochemical performance.

3. Conclusions

The aim of this study was to establish a general understanding of the vacuum post-drying process of whole coils and to enable the design of well-adjusted, application-oriented vacuum post-drying procedures for electrode coils for LIBs. The post-drying parameters have to be adequately chosen to sufficiently reduce the moisture without damaging the sensitive conductive agent/binder systems of the electrodes. This requires a fundamental understanding of structural limitations, heat transfer and water mass transport in the coils. Based on previous experimental studies and theoretical estimations regarding coil heating and removal of water from electrode coils, a comparatively short and moderate 2-phase vacuum post-drying proce-

dure was successfully designed and practically applied. As the material system, an NCM622 cathode (mass loading: 27.1 mg cm^{-2} , density: 3.0 g cm^{-3} , max. coating width: 24 cm), a graphite anode (mass loading: 13.73 mg cm^{-2} , density: 1.5 g cm^{-3} , max. coating width: 24 cm) and Freudenberg separator were used. It was shown that:

1. The most crucial factor for the success of the post-drying procedure is to achieve axial diffusion through half of the coating width to a sufficient scale (requiring a continuous coating over the width, or longitudinal slitting before post-drying in case of multiple parallel coatings). The decisive factors for that are adequately high temperatures and low pressure applied for sufficiently long hold times, as well as a consistently low dew point in the oven, achieved through purging cycles.
2. As the temperature is a limiting factor when post-drying LIB electrodes, the post-drying temperature was set to a moderate, safe level of 80°C , on the basis of previous experimental findings, in this study. To determine the necessary pre-heating time to reach 80°C in the whole coils, heat transfer estimations were made for cathode and anode. On the basis of the estimations, the pre-heating phase (phase I) was set to 2 hours at atmospheric pressure (1 bar). After that, phase II of the post-drying procedure, the actual post-drying phase, was designed. The purging cycles were laid out pursuant to the limitations of the vacuum oven and set to an amplitude from 10 mbar to 30 mbar with a hold time of 10 min at 10 mbar each time. The necessary hold time of phase II was then estimated with the preassigned conditions, on the basis of mass transfer in a cathode coil, and set to 4.7 hours. Altogether, a II-phase vacuum post-drying procedure containing a heating phase ($80^\circ\text{C}/2\text{ h}/$ atmospheric pressure) and a vacuum post-drying phase ($80^\circ\text{C}/4.7\text{ h}/14$ purge cycles between 10 and 30 mbar) was designed
3. The designed post-drying procedure was able to sufficiently reduce the residual moisture of all cell components without deteriorating their structural properties. The total cell moisture content was reduced to 168 ppm, the specific electrical resistance of the cathode decreased by 37% and a good C-rate stability, as well as stable electrochemical long term performance was achieved.
4. Besides proving that the designed procedure was well-adjusted even for wider coatings or longer coils, the measurements of the residual moisture after post-drying showed that a low dew point after post-drying is very important, especially as the anode and the separator remoisten quickly and are very sensitive to fluctuating or higher dew points. The anode, as well as the cathode and the separator, showed hysteresis behavior, so remoistening after post-drying does occur, but to a lower degree than in the Non-PD state. Once the electrode has been dried to lower water activities corresponding to a low relative humidity or rather lower dew points, the level of the adsorption isotherm is deeper and approaches the original moisture level at higher dew points, correspondingly.

Altogether, the results show that post-drying procedures can be designed on the basis of fundamental findings attained in experimental studies, combined with theoretical estimations regarding the drying of residual water from electrode coils, which can be made by describing the heat transfer and water mass transport within the electrode coil. Once the estimations are made and the requirements and limitations of post-drying processes are understood, established post-drying procedures can be easily adjusted for changing demands.

Experimental Section

The goal of this study was to develop a vacuum post-drying procedure which can be adjusted to anodes and cathodes with different coating widths and lengths within the coils. While the temperature was set with regard to the temperature sensitive binder systems of both electrodes on the basis of experimental findings and research (cf. Section 2.1), the process timing was determined with the help of estimations regarding the heat and mass transfer during the vacuum post-drying. By this, reasonable orders of magnitude for the duration of the post-drying process were obtained.

Materials and Electrode Manufacturing Processes

To be able to estimate the universal applicability of the designed procedure, anode and cathode coils with different coating widths and electrode lengths were produced. Before and after post-drying, the remaining moisture content of the coils was measured with coulometric Karl Fischer Titration. To further increase the understanding of the effects of post drying procedures on battery performance, the electrical resistance and electrochemical performance were investigated. The electrodes were formulated with common materials and recipes. The cathodes were produced using 95.5 wt% active material ($\text{LiNi}_{0.6}\text{Co}_{0.2}\text{Mn}_{0.2}\text{O}_2 = \text{NCM}622$, BASF) and 2.25 wt% binder (polyvinylidene fluoride = PVDF, Solef 5130, SOLVAY). As conductive agents, 1.5 wt% carbon black (C-Nergy Super C65, IMERYS) and 0.75% conductive graphite (TIMREX SFG6 L, Imerys) were added. N-Methyl-2-pyrrolidone (NMP, electrochemical grade, BASF) was used as solvent. The anodes were produced with 94 wt% active material (graphite) and 4 wt% binder (2 wt% carboxymethyl cellulose = CMC, CMC Sunrose MAC500LC, Nippon Paper and 2 wt% styrene-butadiene-rubber = SBR). As conductive agent, 2 wt% carbon black (C-Nergy Super C65, IMERYS) were added. Deionized water was used as solvent. For the electrode manufacturing, the same process as in a previous study^[1] was used. The anodes were produced in several batches with a TURBULA® T 2 F mixer (Willy A. Bachofen AG Maschinenfabrik, Switzerland) and a dissolver DISPERMAT CA60 (VMA-Getzmann GmbH, Germany), whereas the cathode was processed in one batch in a planetary mixer PMH10 (NETZSCH GmbH and Co. Holding AG, Germany). For further details see Huttner et al.^[1].

For the identification of the impact created by the post-drying procedure, electrodes with high mass loading were produced. Cathodes were processed with a mass loading of 27.1 mg cm^{-2} and anodes with a mass loading of 13.73 mg cm^{-2} , accordingly. This corresponds to a total cell capacity of 4.4 mAh cm^{-2} . For both electrodes, coating widths of 11 cm and 24 cm were produced. The cathode was coated on a $20 \mu\text{m}$ thick aluminium foil (Hydro Aluminium GmbH, Germany) and compressed to a coating density of 3.0 g cm^{-3} in a calender GKL 400 (SAUERESSIG GmbH und Co. KG, Germany). The anode was coated on a copper foil with a thickness of $10 \mu\text{m}$ (Sumitomo Electric Hartmetall GmbH, Germany)

and calendered to a coating density of 1.5 g cm^{-3} . After calendering, the 24 cm wide coated electrodes were rolled into coils of 10 m (M-coil) each, while for the 11 cm wide coated electrodes three coil lengths (5 m = S-coil, 10 m = M-coil, 20 m = L-coil) were produced. The polyester/ceramic FS 3011-23 (Freudenberg Performance Materials SE & Co. KG) served as separator.

Heat Transfer Estimations

In order to enable appropriate diffusion rates and a low water activity, a sufficiently high coil temperature is necessary. Due to the very limited heating ability in the vacuum state, the battery coil is pre-heated in a first process step at a pressure of $p=1 \text{ bar}$ and a temperature of $T=80^\circ\text{C}$ (the selection of the temperature is explained in chapt. 2.1). In order to evaluate the time period required for the whole coil volume to reach a target temperature, simulations were performed using the COMSOL Multiphysics® program. The high number of very thin layers in the coil requires high calculation costs. Therefore, a simplified 2D simulation model has been developed by implementing a suitable tensor for the thermal conductivity and using mean values for the density and heat capacity. The 2D model was validated by comparing it to several 3-dimensional thin-layer-models of smaller coils consisting of less layers. The heat flux on the coil surface is calculated assuming a constant temperature of the ambience of $T=80^\circ\text{C}$. The heat transfer coefficient α is calculated by the correlation for external natural convection of a long horizontal cylinder of Churchill and Chu [Equation (9)]^[51] and is determined by the thermal conductivity λ , the cylinder diameter D , the Prandtl Number Pr and the Rayleigh number Ra . Archarya and Dash recommended the correlation to calculate the most accurate heat transfer coefficient for horizontal cylinders for a high range of Prandtl and Rayleigh numbers.^[52]

$$\alpha = \frac{\lambda}{D} \cdot \left(0.6 + \frac{0.387 Ra^{1/6}}{\left(1 + \left(\frac{0.559}{Pr} \right)^{9/16} \right)^{8/27}} \right)^2 \quad (9)$$

The calculated heat transfer coefficient α is required as a boundary condition for the solution of the heat transfer equation [Equation (10)]. For the calculation of the heat transport, the initial conditions for the coil [Equation (11)] and the ambience [Equation (12)] are set.

$$\dot{q}|_{r=R} = \alpha \Delta T \quad (10)$$

$$T_{Coil}|_{t=0} = 20^\circ\text{C} \quad (11)$$

$$T_{Amb}|_{t=0} = 80^\circ\text{C} \quad (12)$$

The temporal course of the calculated mean temperature of the coil during the heating process is plotted in Figure 13. At the beginning the coil temperature rises quickly, afterwards it approaches the target temperature of $T=80^\circ\text{C}$ asymptotically. After 2 hours, it has reached a temperature of $T=78^\circ\text{C}$, which can be assessed as sufficiently close to the desired temperature.

Furthermore, it seems interesting to analyze temperature gradients inside the battery coil in order to assess the expressiveness of the considered mean temperature. Therefore, the maximum and minimum temperature inside the coil have been calculated and plotted on the secondary axis as the deviation from the mean value. At the beginning, the differences rise quickly and reach a

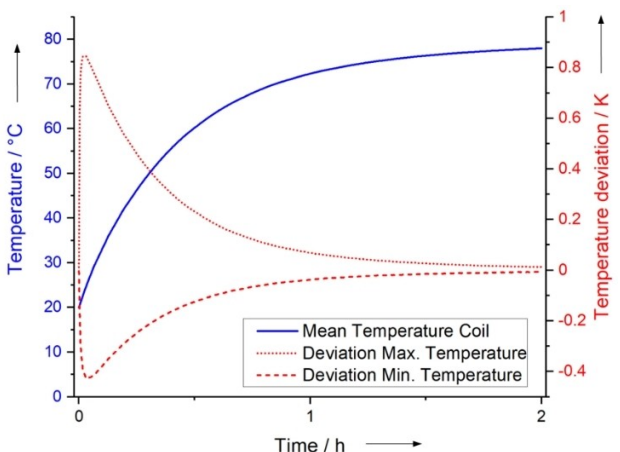


Figure 13. Mean temperature and temperature deviation inside the coil during the atmospheric heating process.

maximum difference between max. and min. temperature of 1.2 K after about 2 minutes. Subsequently, temperature gradients decrease to a negligible value after 120 minutes. In consequence, it can be assumed to start the post-drying process with a homogeneous coil temperature of almost $T=80^{\circ}\text{C}$ after 2 hours heating at atmospheric pressure.

Mass Transfer Estimations

The heat transfer simulation provides an estimation for the necessary duration of the heating period. Similarly, the mass transport simulation estimates the drying time necessary for the system to reach sufficient proximity to the sorption equilibrium. This estimation aims at describing a conservative drying scenario, serving as a reliable basis for establishing an experimental procedure. The one-dimensional mass transport describes the moisture content inside the electrode, which is calculated using equation 4. MATLAB® 2020 serves as software environment and the MATLAB®-native function PDEPE solves the partial differential equations. The simulation domain of the mass transport model requires isothermal conditions to be justified. Therefore, the time-averaged mean temperature of 71.17°C derived from the heat transfer estimation is set throughout the domain for the duration of the heating period. Subsequently, the oven temperature is set to 80°C according to the experimental procedure. The Dirichlet boundary condition is applied for the mass transfer at the interface to the vacuum oven and the Neumann boundary condition is set to the mirror axis (cf. Figure 2). As the dew point depends on the amount of moisture released from the coil as well as the volume of the oven, it was decided to design this vacuum drying process with implemented dry-gas purging cycles. The simulation also incorporates these purging cycles. Accordingly, the dew point inside the oven is estimated to be $T_D=-80^{\circ}\text{C}$. The initial values equal the sorption equilibria at dry room condition which is where the coils rest before post-drying. A cathode sorption equilibrium accounts for material-specific desorption properties. A pressure of 1 bar is maintained during the heating period of two hours. The moisture content decreases to below ten percent of its initial content within 6.7 hours of drying time in both coil geometries (cf. Figure 6). Thus, 6.7 hours of drying time including a 2 hours heating period set the timeframe for the experimental procedure. Based on the findings of the estimations, a post-drying procedure for vacuum ovens was designed that was transferable into experimental application, using the existing lab equipment with its specific limitations.

Post-Drying Procedure

With the help of the findings of previous studies^[1] and the estimated framework conditions, a post-drying procedure was designed according to the existing lab equipment, namely a vacuum oven VD 115 with a pump VAP 1 (final pressure 7 mbar) from BINDER GmbH, Germany and a vacuum controller CVC3000 from VACUUBRAND GmbH und Co KG., Germany. The drawn post-drying procedure (cf. Figure 3) was parted into two phases: The first phase, the heating phase, targets a uniform heating of the whole coil and was conducted under atmospheric pressure, as heat transmission is better at higher pressure. The second phase of the post-drying procedure, the vacuum post-drying phase, was performed under vacuum, including various purging cycles with Argon to remove the released moisture of the vacuum oven in order to maintain a dew point as low as possible. The exact parameters and hold times are listed in Table 1.

In phase I, the coils were heated to the target temperature of 80°C for 2 hours under atmospheric pressure and in dry room air ($T_0=\text{ca. }-45^{\circ}\text{C}$) in the preheated oven. The attainment of the goal temperature inside the coils was validated using temperature measurement stripes (REATEC-AG®, Switzerland), which were placed inside the coils. Phase II of the post-drying procedure, the vacuum post-drying phase, lasted 4.7 hours and was conducted using the vacuum controller, whereby the hold times were chosen according to the limitations of the vacuum pump. After flushing the oven with dry Argon gas (purging step), the vacuum pump needed approximately 7.5 min to achieve the 10 mbar target absolute pressure again. The holding steps were used to achieve a low pressure for good mass transport by increasing the diffusion coefficient, while the purging steps were used to reduce the water content inside the gaseous phase to increase the concentration gradient in the gas phase. After 14 purging cycles, the vacuum oven was flushed with dry Argon gas and the coil was taken out of the oven. The material for the cell assembly and the samples for further analyses were then taken at half of the total coil length.

Determination of Water Content Via Karl Fischer Titration

In order to investigate the effectiveness of the post-drying procedure, samples of the cell components were measured before and after post-drying using a Karl Fischer Titrator AQUA 40.00 with headspace module (ECH Elektrochemie Halle GmbH, Germany). For measuring, the oven temperature of the Karl Fischer Titrator was set to 100°C for the anode, 120°C for the cathode and 100°C for the separator. The measuring time was set to 10 min. The measuring temperatures were set as low as possible to reproduce realistic post-drying conditions on the one hand and to prevent side reactions or oxidation of the current collectors on the other hand.^[16] The lower limit of the temperatures which is needed to reproducibly measure the moisture of the cell components was determined by temperature ramps and comparison of moisture measurements at different temperatures, both conducted with the Karl Fischer Titrator. For each analysis, a threefold determination was conducted and averaged. For further details concerning the measuring method see Huttner et al.^[1]

In this study, the titrator was placed in a dry room with a dew point of $T_D=-25^{\circ}\text{C}$. To ensure that the cell components had already reached the equilibrium with the ambient humidity, all samples were exposed to the respective test environment for 1 hour before crimping. For the comparability of the moisture contents, the results were calculated in parts per million (ppm) according to the following Equation (13).

$$x_{\text{moisture}}[\text{ppm}] = \frac{m_{\text{detected moisture}}[\mu\text{g}]}{m_{\text{sample weight}}[\text{g}]} \quad (13)$$

As the current collectors only absorb marginal amounts of water^[16], the detected moisture was considered to originate from the coating, which is why the proportion of the current collector was subtracted from the measured sample weight before the calculation of the ppm-moisture.

Specific Electrical Resistance

For the investigation of the specific electrical resistance, an in-house developed testing method was used. By the usage of that method it is possible to gain a further understanding of the electron transport kinetics as a function of ohmic resistance or conductance. The testing was conducted with a uniaxial material testing machine (Z020, Zwick GmbH & Co.KG, Germany) which is positioned in a dry room with $T_D = -25^\circ\text{C}$. The electrical resistance was then put into relation to the sample dimensions to calculate the specific electrical resistance of the samples. For each analysis, 10 measurements were conducted and averaged. For further information see Westphal et al.^[53] and Haselrieder et al.^[54].

Electrochemical Characterization

Two sets of one compartment pouch cells with edge lengths of 50 mm (cathodes) and 55 mm (anodes) and a FS 3011-23 separator (Freudenberg Performance Materials SE & Co. KG, 14.5 cm coil width) were built to investigate the electrochemical rate-capability. The first set of pouch cells consisted of components which were post-dried with the designed vacuum post-drying procedure in an M-coil configuration (10 m length within the coil) and 11 cm coating width (only the electrodes). They were shrink-wrapped into impermeable foils after post-drying and transferred into a glovebox (GS Glovebox Systemtechnik GmbH, Germany; $\text{O}_2/\text{H}_2\text{O} < 0.1 \text{ ppm}$) for cell assembly without further exposition to other influences. The second set of cells consisted of cell components which were post-dried with a reference post-drying procedure of previous studies (Argon-PD)^[1], using the pre-switched vacuum lock of the Argon-glovebox. Therefore, the non-post-dried components (electrodes and separator) were placed as single sheets inside the pre-switched vacuum lock and post-dried with an automatic purging program which consists of three vacuum/Argon purging cycles at 20°C with a total time of 15 min. The final vacuum amounted to $< 0.01 \text{ mbar}$ and the purging steps were conducted up to 500 mbar.

LP57 (BASF SE; Germany) with 1 M LiPF₆ and 2 vol% vinylene carbonate was used as electrolyte. The electrochemical characterization was conducted at room temperature (21°C) in a battery testing machine (Series 4000, MacCor, Inc., USA). For each post-drying procedure, 5 cells were assembled and the best 3 cells were used for the analysis of the electrochemical performance. The test procedure is portrayed in Table 2.

Acknowledgements

The authors gratefully thank the German Federal Ministry for Economic Affairs and Energy (BMWi) for the financial support. The IGF project (19985 N) of the Research Association Forschungskuratorium Maschinenbau e.V. (FKM) was funded via the AiF within the framework of the program for the promotion of joint

Table 2. Parameters of the electrochemical testing procedure (cut-off voltages: 3.0 and 4.2 V).	
Cycling step	Charge and discharge parameters
Formation	$3 \times 0.1 \text{ C}/0.1 \text{ C}$ (Ch./Dis) only CC
1. C-rate test	$3 \times 0.2 \text{ C}/0.2 \text{ C}$ (Ch./Dis) CCCV in Ch. $3 \times 0.2 \text{ C}/1.0 \text{ C}$ (Ch./Dis) CCCV in Ch. $3 \times 0.2 \text{ C}/2.0 \text{ C}$ (Ch./Dis) CCCV in Ch. $3 \times 0.2 \text{ C}/3.0 \text{ C}$ (Ch./Dis) CCCV in Ch. $3 \times 0.2 \text{ C}/5.0 \text{ C}$ (Ch./Dis) CCCV in Ch.
Recovery after C-Rate test	$2 \times 0.1 \text{ C}/0.1 \text{ C}$ (Ch./Dis) CCCV in Ch.
Cycling	$50 \times 1.0 \text{ C}/1.0 \text{ C}$ (Ch./Dis) CCCV in Ch.
Recovery before all further C-rate tests	$2 \times 0.1 \text{ C}/0.1 \text{ C}$ (Ch./Dis) CCCV in Ch.
Further C-rate tests	$3 \times 0.2 \text{ C}/1.0 \text{ C}$ (Ch./Dis) CCCV in Ch. $3 \times 0.2 \text{ C}/2.0 \text{ C}$ (Ch./Dis) CCCV in Ch. $3 \times 0.2 \text{ C}/5.0 \text{ C}$ (Ch./Dis) CCCV in Ch.
Recovery after all further C-rate tests	$2 \times 0.1 \text{ C}/0.1 \text{ C}$ (Ch./Dis) CCCV in Ch.

industrial research and development (IGF) by the Federal Ministry of Economics and Technology on the basis of a resolution of the German Bundestag. The authors would also like to thank Laura Jess, Heather Cavers, Tanja Boll, Rainer Severin, Jan-Michael Kröhnke, Alexander Neuberger, Axel Rosenkranz and Stoyan Ivanov for the experimental support and the fruitful discussions. Open access funding enabled and organized by Projekt DEAL.

Conflict of Interest

The authors declare no conflict of interest.

Keywords: diffusion • electrochemistry • lithium-ion batteries • residual moisture • vacuum post-drying

- [1] F. Huttner, W. Haselrieder, A. Kwade, *Energy Technol.* **2019**, *8*, 1900245.
- [2] A. Kwade, W. Haselrieder, R. Leithoff, A. Modlinger, F. Dietrich, K. Droeber, *Nat. Energy* **2018**, *3*, 290.
- [3] J. C. Eser, T. Wirsching, P. G. Weidler, A. Altvater, T. Börnhorst, J. Kumberg, G. Schöne, M. Müller, P. Scharfer, W. Schabel, *Energy Technol.* **2020**, *8*, 1801162.
- [4] J.-H. Schunemann, H. Dreger, H. Bockholt, A. Kwade, *ECS Trans.* **2016**, *73*, 153.
- [5] X. Sun, X. Luo, Z. Zhang, F. Meng, J. Yang, *J. Cleaner Prod.* **2020**, *273*, 123006.
- [6] C. M. v. 't. Land, *Drying in the process industry*, John Wiley & Sons, Hoboken N. J. **2012**.
- [7] M. Wohlfahrt-Mehrens, C. Vogler, J. Garche, *J. Power Sources* **2004**, *127*, 58.
- [8] S. F. Lux, I. T. Lucas, E. Pollak, S. Passerini, M. Winter, R. Kostecki, *Electrochim. Commun.* **2012**, *14*, 47.
- [9] L. Terborg, S. Nowak, S. Passerini, M. Winter, U. Karst, P. R. Haddad, P. N. Nesterenko, *Anal. Chim. Acta* **2012**, *714*, 121.

- [10] T. Kawamura, A. Kimura, M. Egashira, S. Okada, J.-I. Yamaki, *J. Power Sources* **2002**, *104*, 260.
- [11] S. Nowak, M. Winter, *J. Anal. At. Spectrom.* **2017**, *32*, 1833.
- [12] U. Heider, R. Oesten, M. Jungnitz, *J. Power Sources* **1999**, *81–82*, 119.
- [13] U. Langklotz, M. Schneider, A. Michaelis, *J. Ceram. Sci. Tech.* **2013**, *04*, 69.
- [14] C. A. Heck, M.-W. von Horstig, F. Huttner, J. K. Mayer, W. Haselrieder, A. Kwade, *J. Electrochem. Soc.* **2020**, *167*, 160521.
- [15] J. Vetter, P. Novák, M. R. Wagner, C. Veit, K.-C. Möller, J. O. Besenhard, M. Winter, M. Wohlfahrt-Mehrens, C. Vogler, A. Hammouche, *J. Power Sources* **2005**, *147*, 269.
- [16] M. Stich, N. Pandey, A. Bund, *J. Power Sources* **2017**, *364*, 84.
- [17] S. J. An, J. Li, C. Daniel, D. Mohanty, S. Nagpure, D. L. Wood, *Carbon* **2016**, *105*, 52.
- [18] P. Novák, F. Joho, M. Lanz, B. Rykart, J.-C. Panitz, D. Alliata, R. Kötz, O. Haas, *J. Power Sources* **2001**, *97–98*, 39.
- [19] J. Qian, W. Xu, P. Bhattacharya, M. Engelhard, W. A. Henderson, Y. Zhang, J.-G. Zhang, *Nano Energy* **2015**, *15*, 135.
- [20] E. R. Logan, H. Hebecker, A. Eldesoky, A. Luscombe, M. B. Johnson, J. R. Dahn, *J. Electrochem. Soc.* **2020**, *167*, 130543.
- [21] S. N. Bryntesen, A. H. Strømman, I. Tolstorebrev, P. R. Shearing, J. J. Lamb, O. Stokke Burheim, *Energies* **2021**, *14*, 1406.
- [22] J. Yamaki, H. Takatsuji, T. Kawamura, M. Egashira, *Solid State Ionics* **2002**, *148*, 241.
- [23] J. Li, C. Daniel, S. J. An, D. Wood, *MRS Advances* **2016**, *1*, 1029.
- [24] K. Liu, S. Yang, L. Luo, Q. Pan, P. Zhang, Y. Huang, F. Zheng, H. Wang, Q. Li, *Electrochim. Acta* **2020**, *356*, 136856.
- [25] S. Liu, L. Xiong, C. He, *J. Power Sources* **2014**, *261*, 285.
- [26] E. R. Logan, H. Hebecker, A. Eldesoky, A. Luscombe, M. B. Johnson, J. R. Dahn, *J. Electrochem. Soc.* **2020**, *167*, 130543.
- [27] D. Prietzl, T. Teufl, A. T. S. Freiberg, B. Strehle, J. Sicklinger, H. Sommer, P. Hartmann, H. A. Gasteiger, *J. Electrochem. Soc.* **2019**, *166*, A4056-A4066.
- [28] S. Komaba, N. Kumugai, Y. Kataoka, *Electrochim. Acta* **2002**, *47*, 1229.
- [29] M. Haarmann, W. Haselrieder, A. Kwade, *Energy Technol.* **2020**, *8*, 1801169.
- [30] Z. An, Y. Li, R. Xu, F. Dai, Y. Zhao, L. Chen, *Appl. Surf. Sci.* **2018**, *457*, 170.
- [31] H. Fan, Y. Peng, Z. Li, P. Chen, Q. Jiang, S. Wang, *J. Polym. Res.* **2013**, *20*, 1.
- [32] M. Kirchhöfer, J. von Zamory, E. Paillard, S. Passerini, *Int. J. Mol. Sci.* **2014**, *15*, 14868.
- [33] J. C. Eser, B. Deichmann, T. Wirsching, P. G. Weidler, P. Scharfer, W. Schabel, *Langmuir* **2020**, *36*, 6193.
- [34] Z. Jiang, F. Zhao, Y. Guan, Z. Qiu, *Theor. Appl. Mech. Lett.* **2019**, *9*, 120.
- [35] P. Zehner, E. U. Schlünder, *Chem. Ing. Tech.* **1970**, *42*, 933.
- [36] E. N. Fuller, P. D. Schettler, J. C. Giddings, *Ind. Eng. Chem.* **1966**, *58*, 18.
- [37] A. F. Mills, *Int. J. Heat Mass Transfer* **2007**, *50*, 5087.
- [38] P. Liu, M. Zhai, J. Li, J. Peng, J. Wu, *Radiat. Phys. Chem.* **2002**, *63*, 525.
- [39] P. Wedin, C. J. Martinez, J. A. Lewis, J. Daicic, L. Bergström, *J. Colloid Interface Sci.* **2004**, *272*, 1.
- [40] D. Parikh, T. Christensen, J. Li, *J. Power Sources* **2020**, *474*, 228601.
- [41] C. J. Weber, S. Geiger, S. Falusi, M. Roth, *AIP Conference Proceedings* **1597** (2014), 66.
- [42] T.-S. Wei, B. Y. Ahn, J. Grotto, J. A. Lewis, *Adv. Mater.* **2018**, *30*, e1703027.
- [43] Z. Zhao, M. Sun, W. Chen, Y. Liu, L. Zhang, N. Dongfang, Y. Ruan, J. Zhang, P. Wang, L. Dong, Y. Xia, H. Lu, *Adv. Funct. Mater.* **2019**, *29*, 1809196.
- [44] S. L. Morelly, N. J. Alvarez, M. H. Tang, *J. Power Sources* **2018**, *387*, 49.
- [45] G. Ning, B. Haran, B. N. Popov, *J. Power Sources* **2003**, *117*, 160.
- [46] H.-J. Noh, S. Youn, C. S. Yoon, Y.-K. Sun, *J. Power Sources* **2013**, *233*, 121.
- [47] R. Jung, M. Metzger, F. Maglia, C. Stinner, H. Gasteiger, *J. Electrochem. Soc.* **2017**, *164*, A1361-A1377.
- [48] Z. Chen, G.-T. Kim, D. Bresser, T. Diemant, J. Asenbauer, S. Jeong, M. Copley, R. J. Behm, J. Lin, Z. Shen, S. Passerini, *Adv. Energy Mater.* **2018**, *8*, 1801573.
- [49] W. Li, J. N. Reimers, J. R. Dahn, *Solid State Ionics* **1993**, *1993*, 123.
- [50] S. Zheng, C. Hong, X. Guan, Y. Xiang, X. Liu, G.-L. Xu, R. Liu, G. Zhong, F. Zheng, Y. Li, X. Zhang, Y. Ren, Z. Chen, K. Amine, Y. Yang, *J. Power Sources* **2019**, *412*, 336.
- [51] S. W. Churchill, H. H. S. Chu, *Int. J. Heat Mass Transfer* **1975**, *18*, 1049.
- [52] S. Acharya, S. K. Dash, *J. Heat Transfer* **2017**, *139*, 371.
- [53] B. G. Westphal, A. Kwade, *J. Energy Storage* **2018**, *18*, 509.
- [54] W. Haselrieder, S. Ivanov, H. Y. Tran, S. Theil, L. Froböse, B. Westphal, M. Wohlfahrt-Mehrens, A. Kwade, *Prog. Solid State Chem.* **2014**, *42*, 157.

Manuscript received: April 22, 2021

Revised manuscript received: May 31, 2021

Accepted article published: June 1, 2021

Version of record online: June 30, 2021